EXAFS, DFT, light-induced nucleobase binding, and cytotoxicity of the photoactive complex cis-[Ru(bpy)2(CO)Cl]+

EXAFS, DFT, Light-Induced Nucleobase Binding, and Cytotoxicity of the Photoactive Complex cis-$[Ru(bpy)_2(CO)Cl]^+$

Luca Salassa,[†] Tiziana Ruiu,[‡] Claudio Garino,[‡] Ana M. Pizarro,[†] Fabrizio Bardelli,[‡] Diego Gianolio,[‡] Aron Westendorf,[§] Patrick J. Bednarski,[§] Carlo Lamberti,[‡] Roberto Gobetto,*[,‡] and Peter J. Sadler*[,†]

† Department of Chemistry, University ofWarwick, Gibbet Hill Road, Coventry CV4 7AL, United Kingdom.
‡ Department of Chemistry IFM and NIS Centre of Excellence, University of Turin, ViaP.Giuria 7, 10125 Turin, Italy.
§ Institute of Pharmacy,University ofGreifswald, 17487Greifswald,Germany.

Abstract

The aqueous photochemistry of *cis*-$[Ru(bpy)_2(CO)Cl]^+$ (**1**) was investigated at 310 K and under visible light (white) irradiation by NMR and ESI-HR-MS. Complex 1 releases a Cl ligand, coordinates a solvent molecule, and forms the complex *cis*-$[Ru(bpy)_2(CO)(H_2O)]^{2+}$ (**2**). Also, irradiation experiments were performed in the presence of the nucleobase derivatives 9-ethylguanine (9-EtG) and 9-ethyladenine (9-EtA). Formation ofRu-9-EtG adducts was observed after 3 h irradiation byNMR and HR-MS, while only very small amounts of a Ru-9-EtA adduct could be detected by HR-MS. Solution structural datawere obtained byX-ray absorption spectroscopy (XAS) for both **1** and **2**. EXAFS gave a Ru-Cl distance of 2.416(7) Å for **1** and a Ru-O_{H2O} distance of 2.102(6) Å for **2**. DFT and TDDFT were employed to study the photophysical and photochemical properties of **1**. Calculations show that dissociative metal-centered states can be related to the light-induced release of a Cl ligand and subsequent coordination of a solventmolecule. The compound showed no antiproliferative activity in three human carcinoma cell lines (lung, bladder, pancreas) under the testing conditions, either with or without irradiation with UV light.

* Corresponding author. E-mail: p.j.sadler@warwick.ac.uk

Introduction

Ruthenium bipyridyl complexes are well known for their photophysical and photochemical properties, which have been successfully exploited for biomedical and biophysical applications.[1] In particular, their absorption and emission features have been used to investigate the ability of these ruthenium derivatives to interact with biomacromolecules, such as proteins and DNA.[2]

Furthermore, ruthenium complexes show potential as alternatives to platinum derivatives in chemotherapy,[3] and two ruthenium(III) complexes, namely, NAMI-A[3a,4] and KP1019,[5] are in clinical trial. Several Ru(II) bipyridyl complexes have been studied as possible anticancer agents as well. A number of studies indicate that the most lipophilic molecules are often the most cytotoxic and that DNA does not seem to be a target for this family of compounds. Confocal microscopy highlights that ruthenium(II) bipyridyl dyes do not accumulate in the nucleus and that their cellular uptake occurs either by endocytosis or by active transport, depending on the structure of the complex.[6] Inthecaseof E. coli the outer membrane protein OMPF appears to be involved in the transportation of polypyridyl ruthenium complexes into the cells.[7] However, a few cases in which ruthenium polypyridyl complexes are able to bind DNA or DNA bases have been reported.[8] Among these, $[Ru(bpy)_2Cl_2]$ (where bpy = 2,2′-bipyridine) was found to be inactive toward murine and human tumor cell lines, while $[Ru(terpy)Cl_3]$ (where terpy = 2,2′;6′,2″-terpyridine) showed remarkably high cytotoxicity.[9]

To explore further the promising field of metal-based photochemotherapy,[10] we have recently investigated the design of new photoactivatable ruthenium complexes.[11] When irradiated with visible light, these are able to release a coordinated ligand and form a reactive aqua species, which can subsequently bind to DNA bases. Due to their rich photochemistry and synthetic versatility, ruthenium bipyridyl complexes are strong candidates for designing new anticancer prodrugs that can be activated by light excitation. The photoproducts can display different reactivity and cell distribution properties compared to ground-state metal complexes (prodrugs), and therefore light activation can be employed to extend the variety of biomacromolecules targeted by this class of complexes.[4,12] Also photoactivation is able to limit the effects of cytotoxic species to irradiated areas, thus allowing specific tissues to be targeted within an organism.

In this study we describe the structural, photochemical, and nucleobase-binding properties of the ruthenium carbonyl complex cis-$[Ru(bpy)_2(CO)Cl]^+$ (**1**). Complex **1** has been previously studied as a photocatalyst for the water gas shift reaction[13] and for CO_2 photoreduction.[14] Although there has been some disagreement [13,14,16a] on the species formed by light excitation of cis-$[Ru(bpy)_2(CO)Cl]^+$, we found that **1** is able to dissociate one Cl^- and form the aqua photoproduct cis-$[Ru(bpy)_2(CO)(H_2O)]^{2+}$ (**2**), Chart 1.[13] Detailed investigations of the structural and electronic properties of **1** and **2** using a variety of techniques (NMR, IR, MS, UV-visible, XAS, and DFT calculations) were carried out to elucidate the mechanism of ligand photodissociation from **1**. Nucleobase binding experiments with 9-ethylguanine (9-EtG) and 9-ethyl-adenine (9-EtA) using NMR and mass spectrometry both in the dark and under irradiation were performed to investigate whether complex 1 might be a candidate for photoactivated targeting of DNA in cells.

Chart 1. Ruthenium Complexes Studied in this Work

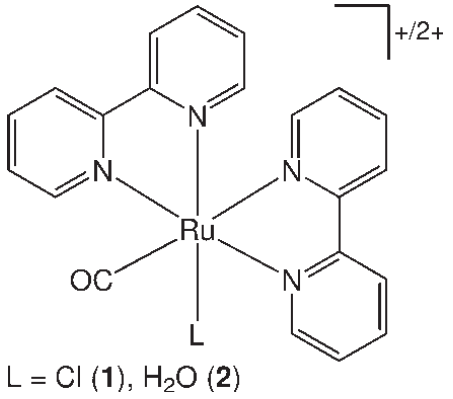

L = Cl (**1**), H_2O (**2**)

Experimental Section

Materials. All solvents and reagents in the synthetic procedures were of analytical/reagent grade and used as received. Ruthenium(III) chloride hydrate was purchased from Lancaster. Lithium chloride, sodium perchlorate, 9-ethylguanine, and 9-ethyladenine were purchased from Aldrich and used without further purification. 2,2′-Bipyridine, obtained from Aldrich, was purified by crystallization from hexane.[15]

Synthesis of *cis*-[Ru(bpy)$_2$(CO)Cl]ClO$_4$, [1(ClO$_4$)]. *cis*-[Ru(bpy)$_2$(CO)Cl]ClO$_4$ was prepared according to slightly modified literature methods.[16] A solution of ruthenium(III) chloride trihydrate (10 g, 38.2 mmol), 2,2′-bipyridine (12 g, 76.9 mmol), and LiCl (11 g) in *N*,*N*-dimethylformamide (60 mL) was refluxed for 8 h under N_2 After cooling at room temperature, the solution was poured rapidly into stirring acetone (300 mL). The resulting mixture was allowed to stand at 273 K overnight. The resultant dark green microcrystalline material, *cis*-[Ru(bpy)$_2$Cl$_2$], was collected on a sintered-glass filter. Complex **1** was obtained by adding sodium perchlorate (1 g) to the mother liquor remaining after the removal of *cis*-[Ru(bpy)$_2$Cl$_2$]. The product was filtered and washed with aliquots of a saturated aqueous solution of sodium perchlorate and then with water (6.6 g, 11.5 mmol, 30% yield based on the ruthenium(III) chloride trihydrate starting material).

^{1}H NMR (D_2O 95%/dmso-d_6 5%, ppm) δ: 7.36 (t, $^3J_{HH}$ = 5.9 Hz, 1H), 7.53 (t, $^3J_{HH}$ = 6.4 Hz, 1H), 7.65 (d, $^3J_{HH}$ = 5.0 Hz, 1H), 7.77 (d, $^3J_{HH}$ = 5.9 Hz, 1H), 7.89 (t, $^3J_{HH}$ = 7.8 Hz, 1H), 7.97 (t, $^3J_{HH}$ = 6.4 Hz, 1H), 8.11 (t, $^3J_{HH}$ = 7.8 Hz, 1H), 8.23 (t, $^3J_{HH}$ = 7.8 Hz, 1H), 8.34 (t, $^3J_{HH}$ = 7.8 Hz, 1H), 8.45 (t, $^3J_{HH}$ = 7.6 Hz, 1H), 8.48 (d, $^3J_{HH}$ = 8.2 Hz, 1H), 8.61 (d, $^3J_{HH}$ = 8.3 Hz, 1H), 8.64 (d, $^3J_{HH}$ = 8.6 Hz, 1H), 8.66 (d, $^3J_{HH}$ = 7.6 Hz, 1H), 9.41 (d, $^3J_{HH}$ = 5.0 Hz, 1H), 9.50 (d, $^3J_{HH}$ = 5.7 Hz, 1H). ^{1}H NMR (CD_2Cl_2, ppm) δ: 7.35 (t, $^3J_{HH}$ = 6.7 Hz, 1H), 7.41–7.45 (m, 2H), 7.67 (d, $^3J_{HH}$ = 4.4 Hz, 1H), 7.71 (td, $^3J_{HH}$ = 6.7 Hz, 1H), 7.81 (td, $^3J_{HH}$ = 6.6 Hz, 1H), 8.04 (td, $^3J_{HH}$ = 7.9 Hz, 1H), 8.09 (td, $^3J_{HH}$ = 7.4 Hz, 1H), 8.18 (td, $^3J_{HH}$ = 7.9 Hz, 1H), 8.31 (td, $^3J_{HH}$ = 7.9 Hz, 1H), 8.36 (d, $^3J_{HH}$ = 8.1 Hz, 1H), 8.37 (d, $^3J_{HH}$ = 7.8 Hz, 1H), 8.41 (d, $^3J_{HH}$ = 8.2 Hz, 1H), 8.49 (d, $^3J_{HH}$ = 8.4 Hz, 1H), 9.33 (d, $^3J_{HH}$ = 5.7 Hz, 1H), 9.68 (d, $^3J_{HH}$ = 5.7 Hz, 1H). ^{13}C NMR (CD_2Cl_2, ppm) δ: 123.6, 124.2, 124.3, 124.4, 127.5, 127.6, 127.7, 128.0, 138.8, 139.4, 139.9, 140.0, 147.9, 151.9, 153.5, 154.8(q), 155.3, 156.3(q), 156.8(q), 156.8(q), 198.77(q). MS: *m*/*z* 477 [M^+]. IR: ν_{CO} 1953 cm^{-1}(ATR), 1965 cm^{-1} (KBr).

Synthesis of *cis*-[Ru(bpy)$_2$(CO)(H$_2$O)](ClO$_4$)$_2$, [2(ClO$_4$)$_2$]. *cis*-[Ru(bpy)$_2$(CO)(H$_2$O)](ClO$_4$)$_2$, was prepared with a slightly modified literature method previously used for ruthenium aqua analogues.[17] The structure of **2** was confirmed by ^{1}H NMR and IR. *Cis*-[Ru(bpy)$_2$(CO)Cl]ClO$_4$ (0.55 g, 1.1 mmol) and AgClO$_4$ (0.48 g, 2.3 mmol) were added to 100 mL of 2:1 acetone/water. The solution was stirred and heated at reflux for 2 hours under N_2, and then allowed to cool to room temperature. The solution was filtered on a sintered-glass filter to remove the AgCl formed during the reaction, and the filtrate was reduced in volume by rotary evaporation. The remaining solution was added to a saturated solution of NaClO$_4$ and a yellow precipitate (complex **2**) formed. The flask was placed in a refrigerator at 277 K for 30 min, and then the yellow product was filtered off and washed with aliquots of cold water (0.53 g, 0.8 mmol, 74% yield). ^{1}H NMR (D_2O, ppm) δ: 7.22 (t, $^3J_{HH}$ = 6.2 Hz, 1H), 7.44 (dd, $^3J_{HH}$ = 5.6 Hz, 1H), 7.59 (d, $^3J_{HH}$ = 5.6 Hz, 1H), 7.64 (d, $^3J_{HH}$ = 4.7 Hz, 1H), 7.82 (t, $^3J_{HH}$ = 5.9 Hz, 1H), 7.91 (t, $^3J_{HH}$ = 6.2 Hz, 1H), 7.99 (t, $^3J_{HH}$ = 8.5 Hz, 1H), 8.17 (t, $^3J_{HH}$ = 8.0 Hz, 1H), 8.28 (t, $^3J_{HH}$ = 8.0 Hz, 1H), 8.37 (d, $^3J_{HH}$ = 7.8 Hz, 1H), 8.39 (t, $^3J_{HH}$ = 7.8 Hz, 1H), 8.53 (d, $^3J_{HH}$ = 8.2 Hz, 1H), 8.56 (d, $^3J_{HH}$ = 8.5 Hz, 1H), 8.59 (d, $^3J_{HH}$ = 8.2 Hz, 1H), 8.92 (d, $^3J_{HH}$ = 5.9 Hz, 1H), 9.49 (d, $^3J_{HH}$ = 4.7 Hz, 1H). IR: ν_{CO} 1966 cm^{-1}(ATR), 1992 cm^{-1} (KBr) and ν_{OH} 3070 cm^{-1}(ATR), 3087 cm^{-1} (KBr).

UV-visible spectroscopy. UV-visible electronic absorption spectra were recorded on a Varian Cary 300 UV-visible spectrophotometer in 1 cm path-length cuvettes. Data were processed with Microcal Origin 8.0.

NMR spectroscopy. NMR spectra were recorded on a Bruker DMX 600 spectrometer (^{1}H operating frequency 600 MHz). ^{1}H NMR spectra were recorded in D_2O, dioxane was added as internal reference (δ = 3.75 ppm) and 5% deuterated dmso to increase the solubility of the complex. The ^{1}H-^{1}H TOCSY and ^{1}H-^{1}H NOESY (phase sensitive) 2D NMR spectra were recorded using standard pulse sequences. The TOCSY mixing time was 60 ms, the NOESY mixing time was 0.50 s.

Infrared spectroscopy. IR spectra were recorded both as a KBr pellet using a Bruker Equinox 55 FT-IR spectrophotometer and as powder-ATR using a Thermo-Nicolet 670 FT-IR spectrophotometer with a resolution of 1 cm^{-1} and an accumulation of 64 scans.

Electrospray ionization high resolution mass spectrometry (ESI-HR-MS). HR-MS data were obtained using a Bruker MicrOTOF mass spectrometer equipped with an electrospray source operating in positive ion mode (ESI+). The *m/z* values reported (scan range: 50−1500 Da) are the strongest in the isotope envelope, and formulae were confirmed by matching isotope patterns with simulated ones generated with Bruker Daltonics DataAnalysis V4.0.

Photochemistry. The light source used was a LZC-ICH2 photoreactor (Luzchem Research Inc.) equipped with a temperature controller and a 16 LZC-VIS UV-visible light lamps (Sylvania cool white, λ = 250–700 nm) with no other sources of light filtration. The temperature was controlled to 310 K unless otherwise stated. The power levels were monitored and assessed using the appropriate probe window, calibrated against an OAI-306 UV power meter from Optical Associates, Inc.; the delivered radiation dose (ca. 1 J/cm^2 h) is defined as irradiance (P, W cm^{-2}) × time (s). HR-MS and NMR spectra in a water/dmso (95%/5%) mixture were then recorded soon after irradiation at different time delays.

Computational Details. All calculations were performed with the Gaussian 03 (G03) program,[18] employing the DFT method. The ground state geometry optimization was performed in the gas phase at two different levels of theory: PBE1PBE[19]/LanL2DZ/6-31G** (**BS1** level) and B3LYP[20]/LanL2DZ/6-31G** (**BS2** level); the LanL2DZ[21] basis set and effective core potential was employed for the Ru atom, while the 6-31G**[22] basis set was used for all other atoms. The lowest-lying triplet state geometry was optimized in the gas phase using the unrestricted Kohn-Sham formalism (UKS).[23] The nature of all stationary points was confirmed by normal-mode analysis.

Thirty-two singlet electronic transitions were calculated by TDDFT,[24] employing the ground state structures optimized at the **BS1** and **BS2** level and including the solvent effect using the CPCM[25] method, with water as solvent. For the TDDFT calculations, either the 6-31G** (**BS1a** and **BS2a**) and the 6-311G**[22] (**BS1b** and **BS2b**) basis sets were employed (6-31G** and 6-311G** were used for the Cl, O, N, C, H atoms, while the LanL2DZ was used for Ru).

The program GaussSum 1.05[26] was used to simulate the electronic spectra of the ruthenium complex and to visualize the singlet excited state transitions as electron density difference maps (EDDMs).[27]

X-ray Absorption Spectroscopy (XAS). EXAFS spectra were acquired on the Dutch beamline at ESRF (BM26-Dubble)[28] at the Ru K-edge (22117 eV) in transmission geometry, using ionization chambers and a fixed-exit monochromator mounting a pair of Si 311 crystals. Energy scans were performed in the range 21690-23350 eV, corresponding to a maximum extension of the EXAFS signal in the *k*-space of 18 $Å^{-1}$. In the edge region (XANES), spectra were sampled with 0.5 eV/point and integration time of 5 s/point; in the EXAFS region the sampling was constant at Δk = 0.05 $Å^{-1}$, and the integration time linearly increased from 4 to 10 s/point from 3 to 18 $Å^{-1}$. Aqueous solutions (10 mM) of **1** and **2** were loaded in cells with different thickness (up to 1.5 cm) in order to obtain a total absorption coefficient between one and two and an edge step close to one. A minimum of five energy scans were acquired for each sample to achieve a high signal-to-noise ratio and averaged after $\chi(k)$ extraction.[29] EXAFS analyses were conducted in the 4–18 $Å^{-1}$ range, starting from structures optimized by DFT calculations. Fits were performed in *k*-space, without Fourier filtering, in order to avoid mathematical artifacts. EXAFS data analysis was performed using the ESTRA and FITEXA software,[30] which is an evolution of the Frascati code.[31] The code exploits the minimization routines of the MINUIT code.[32] Phase and amplitude functions were calculated by FEFF 8.2 code[33] using the structures optimized by DFT calculations as input. Previous work on similar Ru(II) complexes[11c,34] already proved the validity of the phases and amplitudes computed by this approach.

Cell lines. Analyses were carried out using a human urinary bladder carcinoma (5637), a lung carcinoma (A-427) and a pancreas carcinoma (DAN-G) cell lines (German Collection of Microorganisms and Cell

Cultures, DSMZ, Braunschweig, Germany). Cells were grown in medium containing 90% RPMI 1640 medium (Sigma, Taufenkirchen, Germany) and 10% FCS (Sigma), and supplemented with penicillin G (30 mg/L)/streptomycin (40 mg/L). Cells were kept at 310 K in a humidified atmosphere of 5% CO_2.

Antiproliferative activity. Cytotoxicity of **1** was determined by the crystal violet assay.[35] Cells were seeded in 96-well microtiter plates in 100 µL medium at a density of 1000 cells/well and left to adhere overnight. After washing with PBS, the cells were treated with 100 µL of 20 µM solution of **1** in medium (maximum dmso concentration of 0.1%, v/v) and incubated for 1 h. After this time, cells were either irradiated for 30 min with UV light λ = 366 nm or kept in the dark. Luzchem Expo panels (Luzchem Reasearch Inc., Ontario, Canada) were used for UV irradiation. The two Expo panels were accommodated with 5 fluorescent lamps each. Lower UV light was cut off by a filter. The light source was positioned 25 cm away from the samples giving an intensity of 0.12 W/cm^2. Medium removal occurred after 6 hours and the cell survival was determined by using the crystal violet assay. Experiments were performed in triplicate.

Results and Discussion

Structural and Electronic Properties. The X-ray absorption spectra of the chlorido complex **1** and aqua complex **2** were acquired to investigate the solution structures of the complexes and are shown in Figure 1. Data for both complexes could be fitted with structural parameters that are consistent with the computed structures, and in the case of 1 also with the crystal structure.

XANES (X-ray absorption near-edge structure) is sensitive to electronic properties, geometry, and local structure surrounding the absorber atom (ruthenium). The similarity of the two XANES spectra suggests that the substitution of a Cl ligand with a water molecule leaves almost unchanged the local coordination and geometry of all remaining ligands around the metal center. Moreover, the lack of any detectable shift in the absorption edge energy position confirms that ruthenium has the same oxidation state and the same electronic configuration in both **1** and **2**.

The EXAFS (extended X-ray absorption fine structure) signals and the corresponding fit curves for **1** and **2** are reported in Figure 2. Figure 2A reports k^3-weighted EXAFS signal (circles) and fit curves (solid lines). Figure 2B and C report the moduli and the imaginary parts of the corresponding Fourier transforms (FT), which represent the radial distribution function centered on the absorber atom. Each peak in the FT corresponds to an average length (after phase correction) of a single scattering path or to the convolution of more than one path. The first peak (around 1.7 Å) is related to Ru–N distances and to the Ru–C distance involving the CO ligand (Ru-C_{CO}); the second peak at ca. 2 Å, present only in the spectrum of **1**, is associated with the Ru–Cl distance. Conversely, in the spectrum of **2**, the peak associated with the Ru–O distance involving the H_2O ligand is not visible because it is overlapped with the first peak, due to the small difference between the Ru–N and Ru–O bond lengths. Additional peaks at higher R values (2.5–3 Å, uncorrected for phase shift) are related to the Ru–C_{bpy} distances, plus single scattering (SS) of the oxygen atom of the CO ligand and multiple scattering (MS) contributions of the CO ligand (two-body Ru–O–C_{CO} and three-body Ru–C_{CO}–O–C_{CO}–Ru). Additional MS paths involving the bpy carbons (three bodies Ru–C_{bpy}–N) were found to have a relevant contribution to the EXAFS signal and were included in the fits. Contributions beyond 3 Å were not fitted because they do not bring relevant structural information. Moreover, since in the range 3–4.7 Å there are several MS contributions overlapping, it is difficult to obtain reliable fits. The signal beyond 4.7 Å is negligible.

In both k- (Figure 2A) and R-spaces (Figure 2B and C), there is a good correspondence between the experimental and theoretical curves. In the EXAFS spectrum of **2**, the loss of the Ru–Cl contribution (substitution of Cl by H_2O) results in an increase of the first shell signal, due to the fact that Ru–Cl and Ru–O paths are out of phase in a large region of the k-space.[36] This also has little effect on the higher shell signal (2.2–3.5 Å), as well evidenced by the imaginary parts (Figure 2C) of both spectra. Such EXAFS features confirm the XANES observation that the ligand substitution hardly affects both distances and geometries of the CO and bpy ligands.

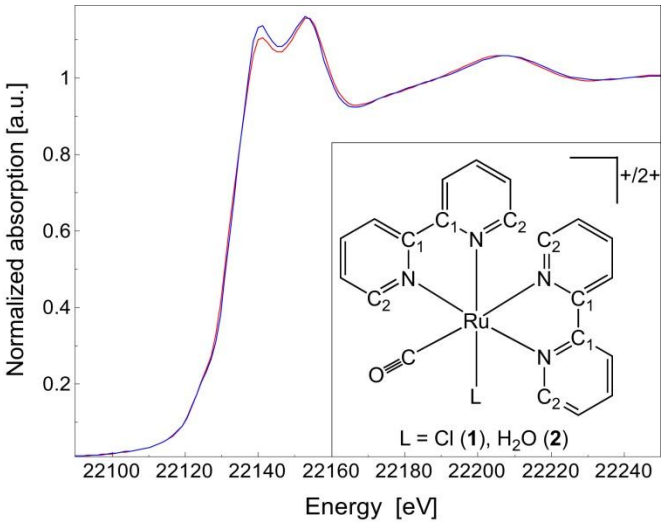

Figure 1. XANES and EXAFS X-ray absorption spectra of **1** (red line) and **2** (blue line). Inset: structural scheme used to construct SS and MS paths for the EXAFS data analysis.

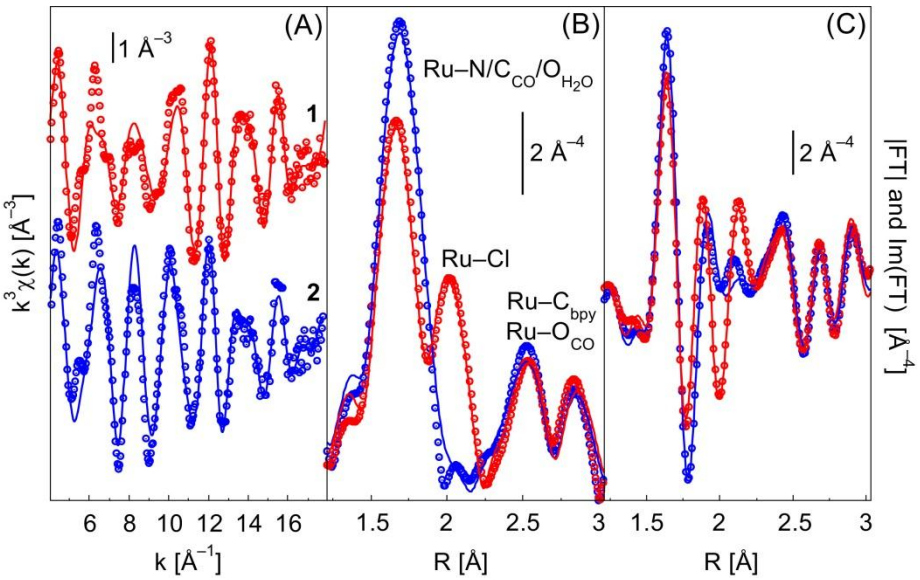

Figure 2. (A) k^3-weighted EXAFS signals (circles) of complexes **1** (red) and **2** (blue), and corresponding best fits (solid lines). (B) k^3-weighted, phase uncorrected, Fourier transform moduli (k-range 4–18 $Å^{-1}$) of the EXAFS signals of fit curves reported in (A). (C) Imaginary parts of the FTs reported in (B). See Supporting information for the k^3-FT spectra plotted up to 5 Å.

The data for complex **1** were fitted by refining 13 independent parameters and for complex **2** with 11. All paths have the same amplitude reduction (S02) and energy shift (ΔE) factors. For complex **2** Ru–O_{H2O} and Ru–N paths were fitted using the same distance parameters and Debye-Waller factors, because the difference in the length is below the resolution limit and EXAFS chemical selectivity is limited to z = ± 4.[37]

Refined structural parameters obtained from the EXAFS fit are reported in Table 1. In cases where the higher shell distance is due to metal carbonyls only, the C–O distance of the CO molecule can also be determined with EXAFS.[38] In the present case and in others successfully solved,[39] the copresence of scattering contributions involving the carbon atoms of the bpy ligands imposes a constraint on the C–O distance to the expected value in the gas phase (1.128 Å).

Structural parameters from DFT were compared to X-ray diffraction (XRD) data for complex **1** only,[16a] while comparison with EXAFS data was performed for both complexes (Table 2). DFT bond distances and angles are in good agreement with XRD data, the only exception being the N2–Ru–Cl angle, which is strongly distorted in the XRD structure due to the crystal packing.[16a] EXAFS data are also in good agreement

with both XRD data and DFT calculations. Considering the lower resolution of EXAFS technique, the three approaches agree on values of the Ru–C_{CO}, Ru–N, Ru–Cl, and Ru–O_{H2O} distances, to within ±0.01, ±0.02, ±0.01, and ±0.02 Å, respectively. For the Ru–N distance, the EXAFS value was compared with the average distances of XRD and DFT approaches ($\langle Ru–N\rangle_{XRD}$ = 2.111 Å and $\langle Ru–N\rangle_{DFT}$ = 2.0965 Å for complex **1**; $\langle Ru–N\rangle_{DFT}$ = 2.0945 Å for complex Å). In all cases the CO ligand binds almost linearly to Ru(II). No significant difference is observed between the two functionals employed; nevertheless the PBE1PBE functional gives slightly better bond distance values (Supporting Information). In the lowest-lying triplet state, **1** shows a distorted geometry where two Ru–N_{bpy} distances are elongated by 0.23 and 0.29 Å compared to the ground-state geometry. Also in the case of **2**, DFT calculations ($\langle Ru–N/O_{H2O}\rangle_{XRD}$ = 2.118 Å) seem to reproduce well the experimental values obtained by EXAFS (2.102 Å).

Table 1. Coordination numbers (*c.n.*), atomic distances (R), and Debye-Waller factors (σ^2) obtained from EXAFS refinements for **1** and **2**.*****

	1			**2**		
Path	*c.n.*	R(Å)	$\sigma^2\cdot10^{-3}$(Å^2)	*c.n.*	R(Å)	$\sigma^2\cdot10^{-3}$(Å^2)
Ru–C_{CO}	1	1.874(8)	2.2(3)	1	1.865(9)	2.8(4)
Ru–N/O_{H2O}	4	2.076(6)		5	2.102(6)	
Ru–Cl	1	2.416(7)	3.2(6)	–	–	–
Ru–C_1(bpy)	4	2.91(1)	1.6(9)	4	2.88(1)	1.1(9)
Ru–C_2(bpy)	4	3.03(1)		4	2.96(1)	
Ru–O_{CO}	1	3.00(1)	1.1(9)	1	2.99(1)	3.1(9)
ΔE	–1(1)			2(1)		
S_0^2	0.74(6)			0.76(6)		
χ_v^2	3.0			4.3		
$<S_0^2,\sigma^2_{Ru–C(CO)}>$	0.84			0.74		
$<\Delta E,Ru–N/O_{H2O}>$	0.81			0.68		

*****The *c.n.* were kept fixed to theoretical values. A common σ^2 parameter for Ru–C_{CO} and Ru–N/O_{H2O}, and for Ru–C_{bpy} paths was employed. Only single scattering paths are reported. Numbers in parenthesis represent the error in the last digit. Also reported are the reduced χ_v^2, the <x,y> are the highest correlations between parameters x and y (all the other being below 0.50 in absolute value).

Table 2. XRD, EXAFS and DFT structural parameters for **1** and **2**.[h]

	1				**2**	
	XRD[a]	EXAFS	DFT - GS[b]	DFT - LL[c]	EXAFS	DFT - GS[b]
			Bond distances (Å)			
C−O	1.122	1.128[d]	1.148	1.146	1.128[d]	1.145
Ru−C_{CO}	1.861	1.874(8)	1.877	1.888	1.865(9)	1.894
Ru−N1	2.097		2.088	2.380		2.087
Ru−N2[e]	2.066	2.076(6)	2.086	2.242		2.054
Ru−N3[f]	2.177		2.129	2.144	2.102(6)	2.132
Ru−N4	2.104		2.083	2.317		2.105
Ru−O_{H2O}	–	–	–	–		2.210
Ru−Cl	2.396	2.416(7)	2.440	2.411	–	–
			Angles (degrees)			
Ru−C−O	174.8	180[g]	177.9	178.6	180[g]	178.8
N2−Ru−Cl	155.3		172.4	164.7		171.3
N1−Ru−N4	167.6		173.3	161.2		172.6
N3−Ru−C	176.5		172.6	174.7		174.9
N1−Ru−N2	78.7		78.1	69.7		78.9
N3−Ru−N4	76.9		77.8	74.1		77.6
N1−C−C−N2	2.7		0.9	11.5		1.1
N3−C−C−N4	-6.4		< 0.1	14.3		1.4

[a] From reference 16a. [b] GS = ground state. [c] LL = lowest-lying triplet state. [d] C−O distance of the CO molecule has been fixed to the value in the gas phase. [e] N trans to Cl or O. [f] N trans to CO. [g] This angle was fixed at 180° in EXAFS refinements. [h] For the EXAFS data, where R values are in merged cells, a single path with higher degeneration has been used in the fitting process.

DFT Calculations and Photophysical Properties. The most significant frontier orbitals of **1** are shown in Figure 3. The HOMO is localized on the Ru–Cl bond (Ru d orbital and Cl p orbital), while the LUMO and LUMO+1 are almost degenerate and centered on the two different bpy ligands. LUMO+6 is a strong σ-antibonding orbital and plays a key role in the photochemical properties of the complex. The lowest-lying triplet of **1** shows two SOMOs with antibonding character (Supporting Information); the lowest-SOMO is a π* Ru–Cl orbital and the highest-SOMO is a σ-antibonding orbital resembling the LUMO+6 of the ground state geometry. The frontier orbitals of **2** in the ground state geometry are similar to the orbitals obtained for **1**.

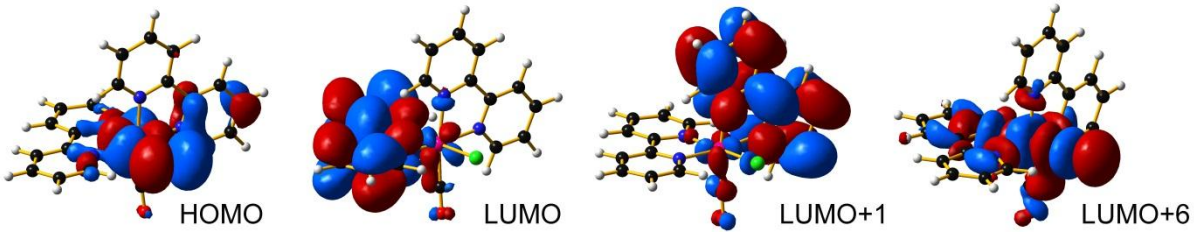

Figure 3. Selected molecular orbitals for complex **1**.

Thirty-two singlet transitions were calculated by TDDFT to assign the UV-visible absorption spectrum of **1**, employing the ground-state structures optimized at the **BS1** and **BS2** level. For each geometry and functional, either the 6-31G** or the 6-311G** basis set were used for the Cl, O, N, C, H atoms (while the LanL2DZ was employed for Ru). No significant difference was found between the calculations; only, a ca. 20-nm red-shift of the two lowest-energy singlet transitions was observed when the B3LYP functional was used and when the 6-311G** basis set was employed.

Figure 4 shows the experimental spectrum for an aqueous solution and the singlet transitions calculated at the **BS1b** level (for the others see Supporting Information). The main absorption band (230–330 nm) contains two sets of singlet transitions. The first set has high oscillator strengths and shows a prevalent metal-to-ligand charge-transfer (MLCT) character; the second set is composed of transitions with major metal-centered (MC) character and lower oscillator strengths. The lowest-energy singlet transitions (> 340 nm) are all MLCT, except one which is MC (360 nm) and has a strongly dissociative character due to the contribution of LUMO+6.

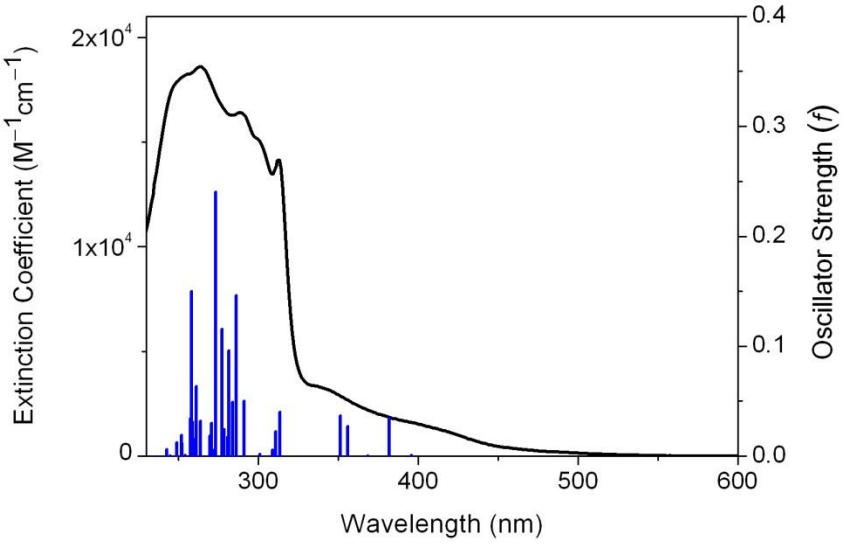

Figure 4. Experimental absorption spectrum (black line) and calculated singlet excited state transitions (blue vertical bars) of **1** in H_2O. The vertical bar height is the oscillator strength.

The lowest-lying triplet state geometry was calculated with the unrestricted Kohn-Sham method.[23] The spin density surface and the SOMOs (Supporting Information) highlight the MC nature of this state, which is consistent with the lack of emission of **1** in several solvents and to its photochemical behaviour.[40]

Photochemistry. As suggested by Tanaka *et al.*,[13] when irradiated in aqueous solution complex **1** undergoes photolysis to form the aqua species *cis*-$[Ru(bpy)_2(CO)(H_2O)]^{2+}$ (**2**). The ^{1}H NMR spectrum in Figure 5 shows that **1** is completely converted into **2** after 3 h of irradiation with white light at ca. 1 J/cm^2 h. During irradiation and conversion of **1** into **2**, the pH of the solution changes from 7.3 to 5.3. Since the pK_a of the Ru–OH_2/OH equilibrium for complex **2** is 8.3,[13] the photo-hydrolysis product believed to prevail in solution is *cis*-$[Ru(bpy)_2(CO)(H_2O)]^{2+}$. Hydrolysis of the Ru–Cl bond occurs also in the dark, however the thermally-activated reaction is significantly slower compared to the photoinduced hydrolysis. In fact, at ca. 310 K twelve hours are required to reach a 50% conversion of **1** (data not shown), while under irradiation the reaction is complete after three hours. Significantly, the ^{1}H NMR spectra of the reaction products obtained by light- and thermal-activation are identical, confirming that in both cases **2** is formed.

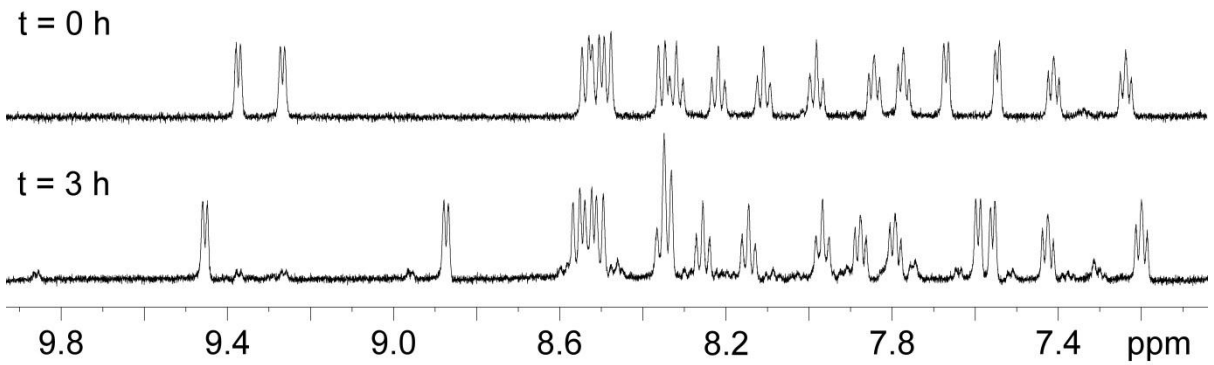

Figure 5. ^{1}H NMR spectrum of **1** in D_2O/dmso-d_6 (95%/5%) solution in the dark (sixteen non-equivalent bpy protons, upper spectrum) and after 3 h of irradiation with white light (lower spectrum), showing the formation of the photoproduct **2** (sixteen non-equivalent bpy protons).

The aromatic region of the ^{1}H NMR spectrum shows all the resonances from the non-equivalent sixteen protons of the two bpy ligands. The two lowest-field doublets can be assigned to the *ortho*-protons of the (bpy) pyridine rings *trans* to each other. This assignment is based on data for $[Os(bpy)_2(CO)(X)]^+$ analogues (where X = Cl, CF_3SO_3 and H).[41]

ESI-HR-MS analysis of the irradiated samples of **1** in solution (95% H_2O/5% dmso) confirmed **2** as a major photoproduct, yielding the molecular formula $C_{21}H_{17}N_4O_2Ru^+$ for the *m/z* = 459 ion (calcd.: 459.0395, found: 459.0398) consistent with $[M - H]^+$. The *m/z* = 477 ion corresponding to remaining complex **1** was also identified (calcd.: 477.0107, found: 477.0053). In addition, a *m/z* = 260 ion corresponding with the molecular formula $C_{23}H_{22}N_4O_2RuS^{2+}$ (calcd.: 260.0248, found: 260.0288) was assigned to the adduct $[Ru(bpy)_2(CO)(dmso)]^{2+}$, which had been previously detected in small quantities by ^{1}H NMR when **1** was irradiated for a prolonged period.

Irradiation of **1** in the presence of 9-ethylguanine, 9-EtG, (ca. 1:1.5 ratio, pH = 6.1) was monitored by ^{1}H NMR. Complex **2** is the major photoproduct, however, formation of Ru-guanine adducts was observed as well (Figure 6). At least two different types of metal-nucleobase adduct are observed as revealed by the presence of two new singlet resonances (blue arrows in Figure 6) at 7.04 and 6.77 ppm. Both these signals can be assigned to the H8 of 9-EtG of two different Ru-guanine adducts, which are present at 16% and 25% in comparison to **2**, as determined from the ^{1}H NMR peak areas. The shift of the H8 signal for these two species is consistent with the shielding effect induced by the ring current of the bpy ligands.[8d] Using 2D ^{1}H-^{1}H TOCSY and NOESY NMR data, it was possible to confirm that the singlet at 6.77 ppm corresponds to a metal-nucleobase species. In particular, a crosspeak between the H8 of 9-EtG and a bpy proton was observed in the NOESY spectrum. Interestingly, when the same solution was left in the dark at 310 K, the ^{1}H NMR

spectrum did not show any formation of Ru-9-EtG adducts, even after 24 h. The presence of two adducts can be ascribed to the loss of CO, possibly caused by prolonged irradiation of the photoproduct **2**. Binding through the N1 of 9-EtG can be ruled out due to steric hindrance (from modelling, not shown). In particular, the singlet at 6.77 can be assigned to the H8 proton of *cis*-$[Ru(bpy)_2Cl(9\text{-}EtG)]^+$, a species previously isolated and crystallized after the hydrolysis of *cis*-$[Ru(bpy)_2Cl_2]$ in the presence of 9-EtG.[8d] Hence it appears that released Cl^- ions can re-coordinate after CO displacement.

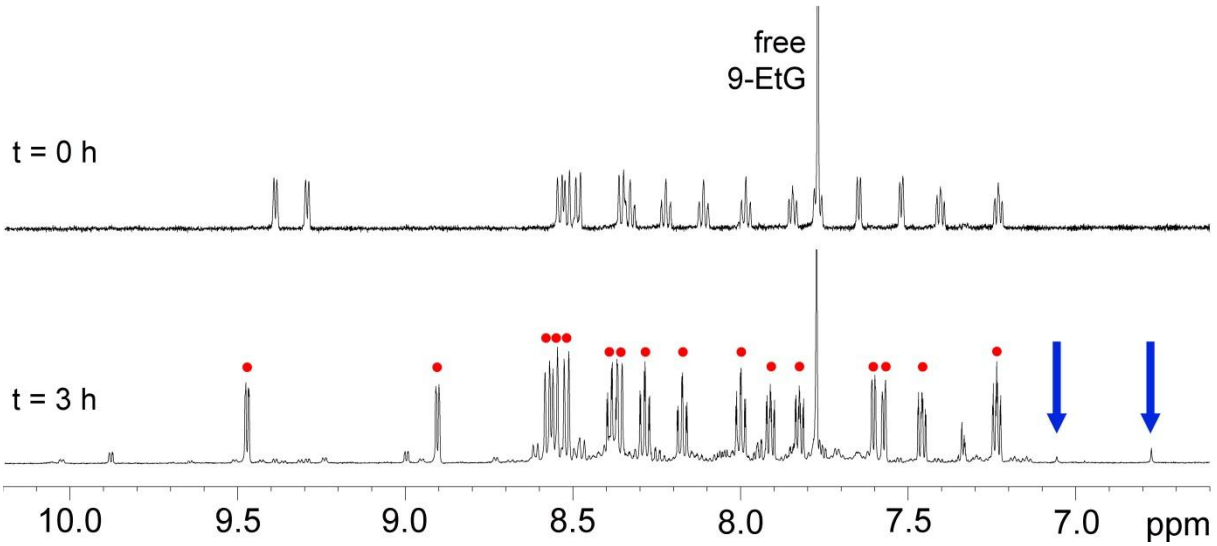

Figure 6. ^1H NMR spectrum of **1** + 9-EtG (1:1.5 ratio) in D_2O/dmso-d_6 (95%/5%) solution in the dark (upper) and after 3 h of irradiation with white light (lower). In the lower spectrum, the ● labels indicate the bpy resonances of *cis*-$[Ru(bpy)_2(CO)(H_2O)]^{2+}$ (**2**), the blue arrows indicate the 9-Et-G H8 resonances of two different metal-nucleobase adducts; a full assignment of the bpy resonances to specific adducts was not attempted due to peak overlap.

When the irradiated solution of **1** and 9-EtG was analyzed by ESI-HR-MS, a major peak was observed in the spectrum corresponding to complex **2** (calcd.: 459.0395, found: 459.0421). Another major ion (*m/z* = 296) yielded the molecular formula $C_{27}H_{25}N_9ORu^{2+}$ (calcd.: 296.5611, found: 296.5583), consistent with the species $\{[Ru(bpy)_2(9\text{-}EtG)]\}^{2+}$, therefore confirming ruthenation of the nucleobase.

Reaction of complex **1** with 9-ethyladenine (9-EtA) was investigated both in the dark (pH = 6.5) and under irradiation. Formation of adducts between the metal complex and the adenine derivative were not observed by ^1H NMR even after six hours of irradiation, while HR-MS data suggested possible formation of a very small amount of a Ru-9-EtA adduct showing a *m/z* = 288 ion, attributable to $\{[Ru(bpy)_2(CO)(9\text{-}EtA)]\}^{2+}$ ($C_{28}H_{25}N_9ORu^{2+}$; calcd.: 288.5636, found: 288.5642).

In view of the finding that light can activate complex **1** toward binding to guanine, a potential nucleobase target in DNA, we investigated the photocytotoxicity of the complex towards three different human carcinoma cell lines.

Antiproliferative activity. Complex **1** was found to be non-toxic to human urinary bladder (5637), lung (A-427) and pancreatic (DAN-G) carcinoma cells in the dark or after 30 min UV irradiation (λ = 366 nm) of cells which had been incubated with 20 μM of **1** for 1 h. The complex did not show any cytotoxic effect at the tested concentration. We can only speculate as to the reasons for this. The complex is positively charged and cell uptake could be low for the incubation time used in the current protocol (1 h). It is possible that even though **1** should be reactive towards DNA when photoactivated, it does not reach DNA. Alternatively, if DNA lesions are formed, then perhaps they are readily excised or repaired, especially if monodentate rather than bidentate adducts are formed. In view of the evidence of the interaction between complex **1** and 9-EtG, and the possibility that DNA adducts might be stable, in future studies it might be worthwhile to investigate cell uptake after longer incubation times.

Conclusions

We have shown that the complex *cis*-$[Ru(bpy)_2(CO)Cl]^+$ (**1**), already known for its photocatalytic properties,[13,14] can release a Cl^- ligand and bind to the nucleobase analogue 9-EtG when irradiated with visible light. NMR and HR-MS confirmed the formation of Ru-9-EtG adducts. Interestingly, in the dark there is no ruthenation of this DNA base although formation of the product *cis*-$[Ru(bpy)_2(CO)(H_2O)]^{2+}$ (**2**) occurs. This suggests that further photoactivation of the aqua species is required for binding to 9-EtG.
For both complexes **1** and **2**, Ru K-edge EXAFS data were in good agreement with both XRD data and DFT calculations. The TDDFT calculations show that LUMO+6 is a strong σ-antibonding orbital and plays a key role in the photochemical properties of the complex. The lowest-lying triplet of **1** shows two SOMOs with metal-centered antibonding character. The presence of this low-lying dissociative ^{3}MC state can be associated with the light-induced release of a Cl ligand and subsequent coordination of a solvent molecule.
Although complex **1** showed no cytotoxic activity towards the human cancer cells used in this study at a concentration of 20 μM, its ability to bind to nucleobases in the presence of light suggests that this class of complexes might provide valuable leads for new photoactivatable antitumor ruthenium complexes.

Acknowledgment

L.S. was supported by a Marie Curie Intra European Fellowship 220281 (PHOTORUACD) within the 7th European Community Framework Programme. C.G. thanks Regione Piemonte for financial support. The EXAFS experiment was performed in the frame of ESRF proposal CH-2948. Dr. S. Nikitenko (ESRF BM26) is acknowledged for the support during collection of EXAFS data. We also thank the members of EC COST Action D39 for stimulating discussions and Drs Ivan Prokes and Lijiang Song of the University of Warwick for their help with NMR and MS instruments, respectively, and Science City AWM/ERDF for support.

Supporting Information

DFT and TDDFT data for **1** and **2**; 2D ^{1}H–^{1}H TOCSY and NOESY of irradiated solutions of **1** in presence of 9-EtG; additional EXAFS data. This material is available free of charge via the Internet at http://pubs.acs.org.

References

1. Lakowicz, J. R., Principles of Fluorescence Spectroscopy. Kluwer Accademic/Plenum Publishers: New York, 1999.
2. (a) Gill, M. R.; Garcia-Lara, J.; Foster, S. J.; Smythe, C.; Battaglia, G.; Thomas, J. A. Nat. Chem. 2009, 1, 662-667; (b) Lim, M. H.; Song, H.; Olmon, E. D.; Dervan, E. E.; Barton, J. K. Inorg. Chem. 2009, 48, 5392-5397; (c) Lo, K. K.-W.; Tsang, K. H.-K.; Sze, K.-S.; Chung, C.-K.; Lee, T. K.-M.; Zhang, K. Y.; Hui, W.-K.; Li, C.-K.; Lau, J. S.-Y.; Ng, D. C.-M.; Zhu, N. Coord. Chem. Rev. 2007, 251, 2292-2310.
3. (a) Alessio, E.; Mestroni, G.; Bergamo, A.; Sava, G., Ruthenium anticancer drugs. In Metal Ions in Biolgical Systems, Vol 42: Metal Complexes in Tumor Diagnosis and as Anticancer Agents, 2004; Vol. 42, pp 323-351; (b) Ang, W. H.; Dyson, P. J. Eur. J. Inorg. Chem. 2006, 4003-4018; (c) Dougan, S. J.; Habtemariam, A.; McHale, S. E.; Parsons, S.; Sadler, P. J. Proc. Natl. Acad. Sci. U. S. A. 2008, 105, 11628-11633; (d) Dougan, S. J.; Sadler, P. J. Chimia 2007, 61, 704-715; (e) Habtemariam, A.; Melchart, M.; Fernandez, R.; Parsons, S.; Oswald, I. D. H.; Parkin, A.; Fabbiani, F. P. A.; Davidson, J. E.; Dawson, A.; Aird, R. E.; Jodrell, D. I.; Sadler, P. J. J. Med. Chem. 2006, 49, 6858-6868; (f) Pascu, G. I.; Hotze, A. C. G.; Sanchez-Cano, C.; Kariuki, B. M.; Hannon, M. J. Angew. Chem.-Int. Edit. 2007, 46, 4374-4378.
4. Alessio, E.; Mestroni, G.; Bergamo, A.; Sava, G. Curr. Top. Med. Chem. 2004, 4, 1525-1535.

5. Hartinger, C. G.; Zorbas-Seifried, S.; Jakupec, M. A.; Kynast, B.; Zorbas, H.; Keppler, B. K. J. Inorg. Biochem. 2006, 100, 891-904.
6. (a) Schatzschneider, U.; Niesel, J.; Ott, I.; Gust, R.; Alborzinia, H.; Wölfl, S. ChemMedChem 2008, 3, 1104-1109; (b) Zava, O.; Zakeeruddin, S. M.; Danelon, C.; Vogel, H.; Grätzel, M.; Dyson, P. J. ChemBioChem 2009, 10, 1796-1800.
7. Ho, M.-Y.; Chiou, M.-L.; Chang, R.-C.; Chen, Y.-H.; Cheng, C.-C. J. Inorg. Biochem. 2010, 104, 614-617.
8. (a) Barton, J. K.; Lolis, E. J. Am. Chem. Soc. 1985, 107, 708-709; (b) Grover, N.; Gupta, N.; Thorp, H. H. J. Am. Chem. Soc. 1992, 114, 3390-3393; (c) Grover, N.; Thorp, H. H. J. Am. Chem. Soc. 1991, 113, 7030-7031; (d) van Vliet, P. M.; Haasnoot, J. G.; Reedijk, J. Inorg. Chem. 1994, 33, 1934-1939; (e) van Vliet, P. M.; Toekimin, S. M. S.; Haasnoot, J. G.; Reedijk, J.; Nováková, O.; Vrána, O.; Brabec, V. Inorg. Chim. Acta 1995, 231, 57-64.
9. Nováková, O.; Kašpárková, J.; Vrána, O.; van Vliet, P. M.; Reedijk, J.; Brabec, V. Biochemistry 1995, 34, 12369-12378.
10. (a) Farrer, N. J.; Salassa, L.; Sadler, P. J. Dalton Trans. 2009, 10690-10701; (b) Angeles-Boza, A. M.; Bradley, P. M.; Fu, P. K. L.; Shatruk, M.; Hilfiger, M. G.; Dunbar, K. R.; Turro, C. Inorg. Chem. 2005, 44, 7262-7264; (c) Ford, P. C. Accounts Chem. Res. 2008, 41, 190-200; (d) Lutterman, D. A.; Fu, P. K. L.; Turro, C. J. Am. Chem. Soc. 2006, 128, 738-739; (e) Mahnken, R. E.; Billadeau, M. A.; Nikonowicz, E. P.; Morrison, H. J. Am. Chem. Soc. 1992, 114, 9253-9265; (f) Moucheron, C. New J. Chem. 2009, 33, 235-245; (g) Patra, A. K.; Bhowmick, T.; Roy, S.; Ramakumar, S.; Chakravarty, A. R. Inorg. Chem. 2009, 48, 2932-2943; (h) Singh, T. N.; Turro, C. Inorg. Chem. 2004, 43, 7260-7262; (i) Turro, C.; Lutterman, D. A.; Liu, Y.; Degtyareva, N. N.; Chouai, A.; Angeles-Boza, A. M.; Dunbar, K. R. Abstracts of Papers of the American Chemical Society 2006, 231, 641-INOR; (j) Mackay, F. S.; Farrer, N. J.; Salassa, L.; Tai, H. C.; Deeth, R. J.; Moggach, S. A.; Wood, P. A.; Parsons, S.; Sadler, P. J. Dalton Trans. 2009, 2315-2325; (k) Mackay, F. S.; Woods, J. A.; Heringová, P.; Kašpárková, J.; Pizarro, A. M.; Moggach, S. A.; Parsons, S.; Brabec, V.; Sadler, P. J. Proc. Natl. Acad. Sci. U. S. A. 2007, 104, 20743-20748; (l) Phillips, H. I. A.; Ronconi, L.; Sadler, P. J. Chem.-Eur. J 2009, 15, 1588-1596; (m) Salassa, L.; Phillips, H. I. A.; Sadler, P. J. Phys. Chem. Chem. Phys. 2009, 11, 10311-10316; (n) Cubo, L.; Pizarro, A. M.; Gomez Quiroga, A.; Salassa, L.; Navarro-Ranninger, C.; Sadler, P. J. J. Inorg. Biochem. 2010, In Press; (o) Schatzschneider, U. Eur. J. Inorg. Chem. 2010, 1451-1467.
11. (a) Betanzos-Lara, S.; Salassa, L.; Habtemariam, A.; Sadler, P. J. Chem. Commun. 2009, 6622-6624; (b) Magennis, S. W.; Habtemariam, A.; Nováková, O.; Henry, J. B.; Meier, S.; Parsons, S.; Oswald, I. D. H.; Brabec, V.; Sadler, P. J. Inorg. Chem. 2007, 46, 5059-5068; (c) Salassa, L.; Garino, C.; Salassa, G.; Nervi, C.; Gobetto, R.; Lamberti, C.; Gianolio, D.; Bizzarri, R.; Sadler, P. J. Inorg. Chem. 2009, 48, 1469-1481.
12. (a) Sanchez-Cano, C.; Hannon, M. J. Dalton Trans. 2009, 10702-10711; (b) Sava, G.; Bergamo, A. Int. J. Oncol. 2000, 17, 353-365; (c) Scolaro, C.; Chaplin, A. B.; Hartinger, C. G.; Bergamo, A.; Cocchietto, M.; Keppler, B. K.; Sava, G.; Dyson, P. J. Dalton Trans. 2007, 5065-5072; (d) Vock, C. A.; Ang, W. H.; Scolaro, C.; Phillips, A. D.; Lagopoulos, L.; Juillerat-Jeanneret, L.; Sava, G.; Scopelliti, R.; Dyson, P. J. J. Med. Chem. 2007, 50, 2166-2175.
13. Ishida, H.; Tanaka, K.; Morimoto, M.; Tanaka, T. Organometallics 1986, 5, 724-730.
14. Fujita, E. Coord. Chem. Rev. 1999, 185-6, 373-384.
15. Amarengo, W. L. F.; Perrin, D. D., Purification of Laboratory Chemicals. 4th ed.; Butterworth-Heinemann: Oxford, U.K., 1996.
16. (a) Clear, J. M.; Kelly, J. M.; O'Connell, C. M.; Vos, J. G.; Cardin, C. J.; Costa, S. R. J. Chem. Soc., Chem. Commun. 1980, 750-751; (b) Lay, P. A.; Sargeson, A. M.; Taube, H.; Chou, M. H.; Creutz, C., Cis-Bis(2,2'-Bipyridine-N,N') Complexes of Ruthenium(III)/(II) and Osmium(III)/(II).

In Inorganic Syntheses, Jean'ne, M. S., Ed. John Wiley & Sons, Inc.: New York, 1986; Vol. 24, pp 291-299.
17. Dobson, J. C.; Helms, J. H.; Doppelt, P.; Sullivan, P.; Hatfield, W. E.; Meyer, T. J. Inorg. Chem. 1989, 28, 2200-2204.
18. Frisch, M. J.; Trucks, G. W.; Schlegel, H. B.; Scuseria, G. E.; Robb, M. A.; Cheeseman, J. R.; Montgomery, J. A., Jr.; Vreven, T.; Kudin, K. N.; Burant, J. C.; Millam, J. M.; Iyengar, S. S.; Tomasi, J.; Barone, V.; Mennucci, B.; Cossi, M.; Scalmani, G.; Rega, N.; Petersson, G. A.; Nakatsuji, H.; Hada, M.; Ehara, M.; Toyota, K.; Fukuda, R.; Hasegawa, J.; Ishida, M.; Nakajima, T.; Honda, Y.; Kitao, O.; Nakai, H.; Klene, M.; Li, X.; Knox, J. E.; Hratchian, H. P.; Cross, J. B.; Adamo, C.; Jaramillo, J.; Gomperts, R.; Stratmann, R. E.; Yazyev, O.; Austin, A. J.; Cammi, R.; Pomelli, C.; Ochterski, J.; Ayala, P. Y.; Morokuma, K.; Voth, G. A.; Salvador, P.; Dannenberg, J. J.; Zakrzewski, V. G.; Dapprich, S.; Daniels, A. D.; Strain, M. C.; Farkas, O.; Malick, D. K.; Rabuck, A. D.; Raghavachari, K.; Forestman, J. B.; Ortiz, J. V.; Cui, Q.; Baboul, A. G.; Clifford, S.; Cioslowski, J.; Stefanov, B. B.; Liu, G.; Liashenko, A.; Piskorz, P.; Komaromi, I.; Martin, R. L.; Fox, D. J.; Keith, T.; Al-Laham, M. A.; Peng, C. Y.; Nanayakkara, A.; Challacombe, M.; Gill, P. M. W.; Johnson, B.; Chen, W.; Wong, M. W.; Gonzales, C.; Pople, J. A. Gaussian 03, Revision C.02; Gaussian, Inc.: Wallingford, CT, 2004.
19. (a) Adamo, C.; Barone, V. J. Chem. Phys. 1999, 110, 6158-6170; (b) Adamo, C.; Scuseria, G. E.; Barone, V. J. Chem. Phys. 1999, 111, 2889-2899.
20. (a) Becke, A. D. J. Chem. Phys. 1993, 98, 5648-5652; (b) Lee, C.; Yang, W.; Parr, R. G. Phys. Rev. B 1988, 37, 785-789.
21. Hay, P. J.; Wadt, W. R. J. Chem. Phys. 1985, 82, 270-283.
22. McLean, A. D.; Chandler, G. S. J. Chem. Phys. 1980, 72, 5639-5648.

23. Vlček, A.; Záliš, S. Coord. Chem. Rev. 2007, 251, 258-287.
24. (a) Casida, M. E.; Jamorski, C.; Casida, K. C.; Salahub, D. R. J. Chem. Phys. 1998, 108, 4439-4449; (b) Stratmann, R. E.; Scuseria, G. E.; Frisch, M. J. J. Chem. Phys. 1998, 109, 8218-8224.
25. (a) Barone, V.; Cossi, M. J. Phys. Chem. A 1998, 102, 1995-2001; (b) Cossi, M.; Barone, V. J. Chem. Phys. 2001, 115, 4708-4717; (c) Cossi, M.; Rega, N.; Scalmani, G.; Barone, V. J. Comput. Chem. 2003, 24, 669-681.
26. O'Boyle, N. M.; Vos, J. G. GaussSum, 1.0; Dublin City University, 2005.
27. (a) Head-Gordon, M.; Grana, A. M.; Maurice, D.; White, C. A. J. Phys. Chem. 1995, 99, 14261-14270; (b) Browne, W. R.; O'Boyle, N. M.; McGarvey, J. J.; Vos, J. G. Chem. Soc. Rev. 2005, 34, 641-663.
28. Silversmit, G.; Vekemans, B.; Nikitenko, S.; Bras, W.; Czhech, V.; Zaray, G.; Szaloki, I.; Vincze, L. J. J. Synchrot. Radiat. 2009, 16, 237–246.
29. Lamberti, C.; Bordiga, S.; Arduino, D.; Zecchina, A.; Geobaldo, F.; Spano, G.; Genoni, F.; Petrini, G.; Carati, A.; Villain, F.; Vlaic, G. J. Phys. Chem. B 1998, 102, 6382-6390.
30. Meneghini, C.; Bardelli, F.; Mobilio, S. http://webusers.fis.uniroma3.it/~meneghini/software.html.
31. Comin, F.; Incoccia, L.; Mobilio, S. INFN Frascati Laboratory Internal Report LNF-82/019(NT), INFN: Rome, Italy, 1982.
32. James, F.; Winkler, M. MINUIT - CERN library, 2004.
33. Ankudinov, A. L.; Nesvizhskii, A. I.; Rehr, J. J. Phys. Rev. B 2003, 67.
34. (a) Salassa, L.; Borfecchia, E.; Ruiu, T.; Garino, C.; Gianolio, D.; Gobetto, R.; Sadler, P. J.; Cammarata, M.; Wulff, M.; Lamberti, C. Inorg. Chem. 2010, 49, DOI:10.1021/ic102021k; (b) Salassa, L.; Gianolio, D.; Garino, C.; Salassa, G.; Borfecchia, E.; Ruiu, T.; Nervi, C.; Gobetto, R.; Bizzarri, R.; Sadler, P. J.; Lamberti, C. J. Phys.: Conf. Series 2009, 190, 012141.
35. Bracht, K.; Boubakari; Grunert, R.; Bednarski, P. J. Anti-Cancer Drugs 2006, 17, 41-51.

36. (a) Leofanti, G.; Padovan, M.; Garilli, M.; Carmello, D.; Zecchina, A.; Spoto, G.; Bordiga, S.; Palomino, G. T.; Lamberti, C. J. Catal. 2000, 189, 91-104; (b) Prestipino, C.; Bordiga, S.; Lamberti, C.; Vidotto, S.; Garilli, M.; Cremaschi, B.; Marsella, A.; Leofanti, G.; Fisicaro, P.; Spoto, G.; Zecchina, A. J. Phys. Chem. B 2003, 107, 5022-5030.
37. Scheinost, A. C.; Kirsch, R.; D., B.; Fernandez-Martinez, A.; Zaenker, H.; Funke, H.; Charlet, L. J. Contam. Hydrol. 2008, 102, 228-245.
38. (a) Lamberti, C.; Palomino, G. T.; Bordiga, S.; Berlier, G.; D'Acapito, F.; Zecchina, A. Angew. Chem.-Int. Edit. 2000, 39, 2138-2141; (b) Prestipino, C.; Capello, L.; D'Acapito, F.; Lamberti, C. Phys. Chem. Chem. Phys. 2005, 7, 1743-1746.
39. Chavan, S.; Vitillo, J. G.; Groppo, E.; Bonino, F.; Lamberti, C.; Dietzel, P. D. C.; Bordiga, S. J. Phys. Chem. C 2009, 113, 3292-3299.
40. Caspar, J. V.; Meyer, T. J. Inorg. Chem. 1983, 22, 2444-2453.
41. Gobetto, R.; Nervi, C.; Romanin, B.; Salassa, L.; Milanesio, M.; Croce, G. Organometallics 2003, 22, 4012-4019.